Organic Electronics 13 (2012) 1204–1212

Contents lists available at SciVerse ScienceDirect

Organic Electronics

journal homepage: www.elsevier.com/locate/orgel

Oligothiophene dendron-decorated squaraine dyes: Synthesis, thin film formation, and performance in organic solar cells

William Kylberg [a], Ying Zhang [c], Arthur Aebersold [a], Fernando Araujo de Castro [b], Thomas Geiger [a], Jakob Heier [a], Simon Kuster [a,1], Chang-Qi Ma [c,*,2], Peter Bäuerle [c], Frank Nüesch [a], Jean-Nicolas Tisserant [a], Roland Hany [a,*]

[a] Empa, Swiss Federal Institute for Materials Science and Technology, Laboratory for Functional Polymers, Überlandstrasse 129, CH-8600 Dübendorf, Switzerland
[b] National Physical Laboratory, Hampton Road, Teddington, Middlesex TW11 0LW, United Kingdom
[c] Institut für Organische Chemie II und Neue Materialien, Universität Ulm, Albert-Einstein-Allee 11, D-89081 Ulm, Germany

ARTICLE INFO

Article history:
Received 2 February 2012
Received in revised form 13 March 2012
Accepted 17 March 2012
Available online 7 April 2012

Keywords:
Organic photovoltaics
Squaraine dye
Donor–acceptor dye
Oligothiophene dendron

ABSTRACT

Squaraine (SQ) dye-based organic semiconductor hybrids 6T-SQ and 18T-SQ functionalized with oligothiophene dendrons were synthesized via Suzuki–Miyaura coupling. The electronic coupling between the oligothiophene dendrons and the squaraine core was rather weak, as suggested from UV–vis spectra, cyclic voltammetry measurements and molecular modeling. Thin films of pure SQ were characterized by a pronounced solvent- and heat-induced crystallization tendency. The dendrons substantially hindered the squaraine core crystallization, and 18T-SQ films remained amorphous after annealing or storage for several weeks. PCBM disrupted dye crystallization in blends, and smooth and stable films could be coated. Heat treatment of blended films induced dewetting for SQ:PCBM and 6T-SQ:PCBM, but 18T-SQ:PCBM remained again stable. These morphological film features could consistently explain the performance of dye-fullerene solar cells. The best performance ($\eta \sim 1.5\%$) was obtained for simple bilayer 6T-SQ:C_{60} or 18T-SQ:C_{60} cells without annealing. Our results demonstrate that the attachment of decorating moieties to a central light-absorbing core unit in molecular push–pull systems can be used to adjust the optoelectronic and morphological film properties of small molecular semiconductors with a strong tendency towards crystallization.

1. Introduction

Solution-processed organic photovoltaic (OPV) cells are receiving considerable attention in the academic and industrial community due to their potential as low-cost and lightweight devices for renewable energy applications [1]. Polymer solar cells are still leading the field [2], but recent work has demonstrated a recurring interest in soluble small organic molecules as electron donor materials [3,4]. Indeed, small molecules present some advantages over polymers, such as ease of synthesis, monodispersity and purification [5]. On the other hand, film forming properties and control over the nanoscale morphology of the active components, which are keys for efficient charge generation and transport, are often challenging [3]. For molecular blend films coated from solution, the morphology develops during solvent evaporation. A quench into the unstable region often initiates spontaneous phase separation. That competes with the crystallization of the individual compo-

* Corresponding authors. Address: Empa, Überlandstr. 129, CH-8600 Dübendorf, Switzerland. Tel.: +41 58 765 4084; fax: +41 58 765 4012 (R. Hany).
E-mail addresses: cqma2011@sinano.ac.cn (C.-Q. Ma), roland.hany@empa.ch (R. Hany).
[1] Present address: ETH Zürich, Institute for Food, Nutrition and Health, Schmelzberstr. 9, CH-8092 Zürich, Switzerland.
[2] Present address: Printable Electronics Research Center, Suzhou Institute of Nano-Tech and Nano-Bionics CAS, 398 Ruoshui Road SEID SIP, Suzhou 215123, PR China.

1566-1199/$ - see front matter © 2012 Elsevier B.V. All rights reserved.
http://dx.doi.org/10.1016/j.orgel.2012.03.022

nents once the solubility limits are crossed and nucleation sites are present or the energy barriers for homogeneous nucleation can be overcome. These films rarely show equilibrium morphologies and further annealing cannot be looked at independently of the coating history.

Power conversion efficiencies (η) of small molecule OPV devices based on oligothiophenes, fused polycycles and various dyes are rapidly increasing, and η = 4.4% (using a dithieno-diketopyrrolopyrrole donor derivative [6]), η = 4.3% (using a star-shaped triphenylamine-benzothiadiazole–oligothiophene donor [7]), or η = 5.08% (using a linear oligothiophene with electron withdrawing cyanoacetate groups [8]) have been reported only recently. These and many other semiconducting small molecules are examples of push–pull architectures, where electron rich and electron poor moieties have been combined to produce molecular donor materials with broad absorptions, increased solubility and tunable redox energy levels [3,9–11].

Using the same design strategy, we report here on the synthesis of oligothiophene dendron functionalized squaraine dye hybrids, and present results on the film formation behavior and performance in organic solar cells using these donor–acceptor–donor (D–A–D) type molecules. Linear, branched and star-shaped oligothiophenes have emerged as a very important materials class for optoelectronic device applications, since their properties can be tuned by chemical modifications, and further functionalization with active molecules is readily possible [12]. Squaraines are 1,3-substituted derivatives of a central electron withdrawing squaric acid core with electron rich aromatic and heterocyclic groups. Squaraine dyes have a good photochemical, thermal, oxygen and moisture stability, and absorb light strongly in the visible and near-infrared region. Squaraines have been successfully used for dye-sensitized solar cells [13,14] and OPV devices [15–23] with, for example, a reported η = 5.2% for a squaraine: fullerene bulk heterojunction solar cell [21]. Details on the performance of these squaraine OPV cells will be presented in the discussion section.

2. Experimental

Materials and methods for the chemical synthesis are described in the electronic supplementary information (ESI) section. Glass (for film morphology studies) and glass/ITO (Thin Film Devices, 140 nm, resistivity 15 ohms square^{-1}, for fabrication of solar cells) substrates were cleaned before spin coating a ~70 nm thick PEDOT:PSS layer, followed by heating at 100 °C for 15 min (poly(3,4-ethylenedioxythiophene):poly(styrenesulfonate), Sigma–Aldrich, conductivity 1 S cm^{-1}). Solutions of pure dyes and blend mixtures with PCBM ([6,6]-phenyl-C_{61}-butyric acid methyl ester, Solenne B.V.) were filtered (0.45 μm) before spin coating on PEDOT:PSS. Film thicknesses were measured on an Ambios XP-1 profilometer. Identical UV–vis spectra for as-prepared solutions and redissolved spin-coated films after heating confirmed that no dye degradation was induced upon film annealing. Annealing experiments (always for 30 min) were carried out on a digitally controlled hotplate inside the glove box. The actual film temperature was estimated by measuring the temperature on the surface of a glass/ITO sample with a contact thermometer. Films for UV and AFM experiments were annealed at ~150 °C, solar cells at ~120 °C or ~150 °C, respectively.

Cyclic voltammetry experiments were performed with a computer-controlled Autolab PGSTAT30 potentiostat in a three-electrode single-compartment cell (5 mL). The working electrode consisted of a platinum wire sealed in a soft glass tube with a surface area of 0.79 mm^2, which was polished down to 0.5 μm with Bühler polishing paste prior to use in order to obtain reproducible surfaces. The counter electrode consisted of a platinum wire and as reference an Ag/AgCl secondary electrode was used.

DSC was carried out under nitrogen on a Perkin Elmer DSC8000 Differential Scanning Calorimeter. Samples were measured with the temperature programme (always 20 °C min^{-1}) of (i) heating from 20 °C to 220 °C, (ii) cooling to 20 °C, (iii) heating to 220 °C. The first heating cycles were ignored to rule out an influence of the thermal history of the samples. For the pure materials between ~0.4 and 3.7 mg were weighed in aluminium pans. For SQ:PCBM blends, $CHCl_3$ solutions containing a total of 1 wt.% SQ and PCBM were added dropwise to the pan until the solid content was ~7 mg. Before DSC measurement, blend samples were dried over night. The fraction of PCBM in the blend was varied between 10% and 90% (w/w%).

Solar cells were fabricated and stored inside a glove box (H_2O < 1 ppm, O_2 < 5 ppm). As cathode, Al (~40 nm, Cerac, 99.999%) was deposited by thermal sublimation under vacuum at a pressure of ~3×10^{-6} mbar through a shadow mask to define solar cells with diameters of 0.2 cm or 0.3 cm, respectively. For bilayer devices, C_{60} (~40 nm, SES Research, 99.9%) and Alq_3 (~2.5 nm, Sigma–Aldrich, 99.995%) were deposited by thermal sublimation between the dye layers and the cathode. Current–voltage (*J*–*V*) characteristics were measured under simulated solar irradiation using the spectrum of a 300 W Xe lamp together with an AM1.5G filter set. A monochromator was used together with the Xe lamp to measure the incident photon-to-current conversion efficiency (IPCE). AFM measurements were performed on a Nanosurf Mobile S in tapping mode at a resonance frequency of 170 kHz using silicon cantilevers. Images were analysed with the WSxM scanning microscopy software.

Density functional theory (DFT) was used to investigate the molecular structure and electron density distribution of the dendronized derivatives. With the exchange and correlation functional B3LYP [24] and the 6-31G* molecular orbitals basis set, calculations were performed using the NWChem 5.1 [25] program installed on the Ipazia computing cluster (http://www.ipazia.ch). NWChem log-files were analyzed with the program Jmol (Jmol: an open-source Java viewer for chemical structures in 3D) and VMD 1.9 [26]. Calculated structures and frontier orbitals were illustrated with POV-ray (Persistence of Vision Pty. Ltd. (2004), Persistence of Vision Raytracer, version 3.7). Chemical structures were optimized for starting conformations with the maximum number of 1,4-trans connected thiophene groups in the dendrons.

3. Results

The synthesis of the squaraine starting compound SQ, SQ-Br2 [27] and the oligothiophene dendrons B-3T-Si and B-9T-Si [28] has been described previously (Scheme 1, Reagents and conditions: i) and ii) Pd_2 $(dba)_3$ $CHCl_3$, HP $(t\text{-}Bu)_3BF_4$, K_2CO_3, THF, 60 °C, overnight; iii) and iv) TBAF/THF, rt, 30 min). Suzuki–Miyaura coupling of SQ-Br2 with the thiophene pinacol boronic esters gave the squaraine oligothiophene hybrids 6T-SQ-Si and 18T-SQ-Si. The trimethylsilyl groups were then removed with tetrabutylammonium fluoride which produced 6T-SQ and 18T-SQ. All compounds were readily soluble in organic solvents such as THF, chloroform or chlorobenzene. Details on the chemical synthesis and characterization are given in the ESI section.

3.1. Optical and film forming properties

The absorption spectrum of SQ (Fig. 1a) showed the typically high molar extinction coefficient ($\varepsilon = 2.76 \times 10^5$ L mol^{-1} cm^{-1}, Table 1) for the main transition at 638 nm and a small vibronic shoulder [29,30]. For the 6T-SQ-Si and 6T-SQ hybrids, the main absorption was bathochromically shifted by more than 40 nm and additional absorption maxima between 300 and 500 nm developed which can be attributed to the 6T dendron units [31]. By extending the dendrons to 18 thiophene units (18T-SQ-Si and 18T-SQ), the short wavelength absorption of the dendron units increased while the long wavelength absorption of the dye core changed marginally. With increasing size of the dendron, the Stokes shift, $\lambda_s = \lambda_{fl}^{max} - \lambda_{abs}^{max}$, only increased from 146 cm^{-1} to 291 cm^{-1} indicating that the structures of the molecules remain largely unchanged during excitation (Table 1).

For a fully conjugated squaraine hybrid system, only one absorption band is expected in the UV–vis spectrum independent of the size of the molecule. Here, the appearance of two absorptions indicates a rather weak electronic coupling between the oligothiophene dendrons and the squaraine core. Optimized structures for the hybrids using molecular modeling support this assumption of restricted effective π-conjugation. Fig. 2 illustrates the optimized structures for 6T-SQ and 18T-SQ. The structure of the squaraine core is completely flat for both hybrids. The thiophene moieties covalently bound to the dye are slightly distorted by 25° (6T-SQ) and 14° (18T-SQ) with respect to the core plane. In turn, further thiophene moieties are more and more distorted. Distortion hinders the effective overlap of the π-orbitals of dye and dendrons and, in both the ground and excited states, electrons are mainly located on the dye core (ESI). This confirms the experimental observation of two separate absorptions, one for the squaraine and one for the dendrons, with a bathochromic shift of the dye maximum in the hybrids.

Cyclic voltammetry was measured in dichloromethane solution. Measurements were referenced against the Fc^+/Fc couple for which an energy level of −5.10 eV *vs.* vacuum was assumed [32,33]. The SQ dye showed two characteristic strong and reversible oxidation waves at ~0 and ~0.49 V (Fig. 3a) [34]. The oligothiophene dendron peaks are expected at potentials higher than +0.5 V and generally manifest only as ill-defined shoulders in the voltammogram [35,36]. For 18T-SQ-Si and 18T-SQ (Fig. 3b), the first dendron oxidation peak overlapped with the second oxidation peak of the squaraine moiety. One reduction wave was observed for all dyes. The small change in the peak

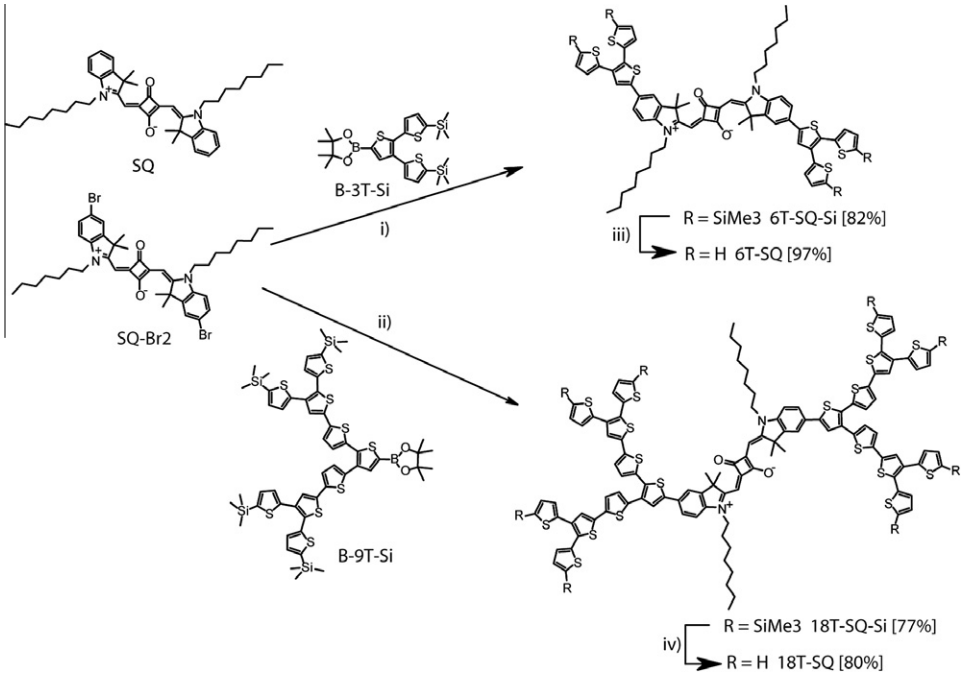

Scheme 1. Synthesis of squaraine oligothiophene hybrids.

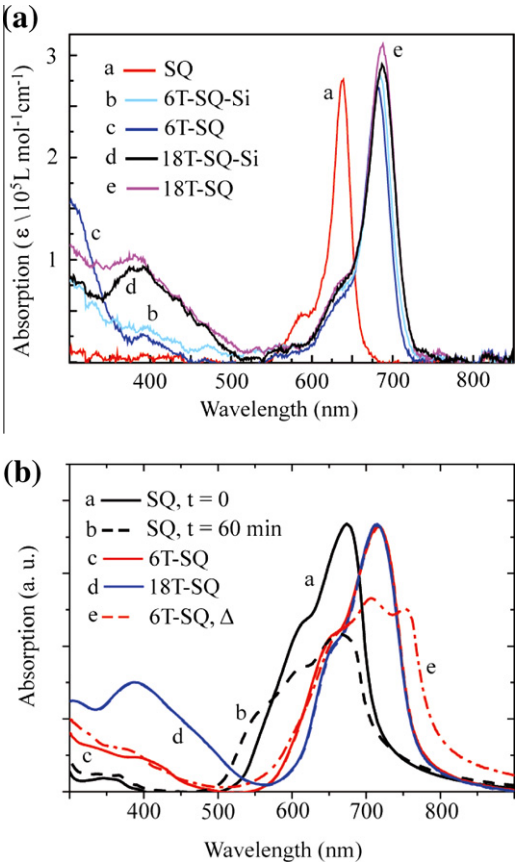

Fig. 1. (a) Absorption spectra in CH_2Cl_2. (b) Absorption spectra of spin-coated thin films from $CHCl_3$ solution (8 mg mL^{-1}) onto PEDOT:PSS. SQ was measured immediately after coating (a, black solid line) and after storing for 1 h under nitrogen at rt (b, dotted black line). 6T-SQ, △ (e, dotted red line) was measured after heating a 6T-SQ film (c, red solid line) at ~150 °C for 30 min. (For interpretation of the references to colour in this figure legend, the reader is referred to the web version of this article.)

positions of the squaraine hybrids with respect to the non-derivatized SQ again confirms that conjugation of the dendronic units with the squaraine core is rather small. The first half-wave oxidation potential ($E_{1/2,ox}$) and the reduction potential ($E_{1/2,red}$) of the cyclic voltammograms was assumed to correspond to the HOMO and the LUMO levels of the dyes (Table 1).

The absorption spectra of spin-coated films (Fig. 1b) were considerably broadened and extended to longer wavelengths (by 26–37 nm, Table 1) than the solution spectra. This can be explained with strong intermolecular interactions and increased molecular ordering in the solid state [37]. When films were stored at room temperature (rt) under nitrogen, the absorption of 6T-SQ and 18T-SQ remained unchanged (spectra c, d in Fig. 1b). However, the absorption of SQ changed considerably during the first hour after spin coating (spectrum a → b in Fig. 1b). The intensity of the main transition reduced and a shoulder at ~550 nm developed. This can be ascribed to solvent-induced reorganization of SQ into more stable crystallites and dimers/H-aggregates due to $CHCl_3$ remaining in the film after coating [19,38].

For longer storage times than ~1 h under nitrogen at rt, the absorption of SQ remained constant as well. The spectral intensity continuously decreased further when the SQ film was heated (data not shown). For the same annealing conditions, the 18T-SQ spectrum remained almost constant, whereas 6T-SQ showed an intermediate behavior between SQ and 18T-SQ. The 6T-SQ film developed a visually inhomogeneous appearance (see below), with unchanged regions and an associated absorption spectrum corresponding to the one at rt (spectrum c, Fig. 1b), and coarsened areas that show a red-shifted absorption peak at ~760 nm (spectrum e, Fig. 1b) indicative of aggregate formation [19,39].

These results demonstrate that the molecular ordering and aggregation behavior between SQ and the squaraine oligothiophene hybrids is substantially different. The rapid solvent removal during spin coating appears to freeze a predominantly amorphous phase morphology for SQ, which crystallizes upon thermal or solvent annealing. For 6T-SQ, the crystallization tendency during film formation is restricted, and largely suppressed in 18T-SQ.

AFM and optical microscope images gave further insight into the film morphology. As-coated films of the plain materials resulted in stable, smooth and featureless (root

Table 1
Optical and redox data of the squaraine core and SQ oligothiophene hybrids.

Compound	Optical data					Electrochemical data[b]				
	λ_{abs}^{max} (nm)[a]	$\varepsilon/10^5$ (L mol^{-1} cm^{-1})	λ_{fl}^{max} (nm)[a]	E_g^{opt} (eV)[c]	$\lambda_{abs}^{max\ film}$ (nm)	$E_{1/2,ox}$ (V)[d]	$E_{1/2,red}$ (V)[d]	E_{HOMO} (eV)[e]	E_{LUMO} (eV)[f]	E_g^{el} (eV)[g]
SQ	638	2.76	644	1.89	675	−0.03	−1.76	−5.07	−3.34	1.73
6T-SQ-Si	684	2.78	696	1.73	708	0.06	−1.65	−5.16	−3.45	1.71
6T-SQ	681	2.68	692	1.73	717	0.06	−1.63	−5.16	−3.47	1.69
18T-SQ-Si	687	2.91	701	1.72	706	0.01	−1.71	−5.11	−3.39	1.72
18T-SQ	687	3.08	701	1.72	713	0.04	−1.69	−5.14	−3.41	1.73

[a] In CH_2Cl_2, rt.
[b] Measured by cyclic voltammetry, in CH_2Cl_2, 1×10^{-3} M, rt, referenced *vs.* Fc^+/Fc.
[c] Calculated from $E_g^{opt}(eV) = 1240/\lambda_{abs}^{onset}(nm)$.
[d] Half-wave potential $E_{1/2} = (E_{pc} + E_{pa})/2$, with the cathodic and anodic peak potentials, E_{pc} and E_{pa}. $E_{1/2,ox}$ is the first half-wave oxidation potential, $E_{1/2,red}$ is the half-wave reduction potential.
[e] Calculated from $E_{HOMO}(eV) = -5.1\ eV - e\ E_{1/2,ox}$, *vs.* Fc+/Fc.
[f] Calculated from $E_{LUMO}(eV) = -5.1\ eV - e\ E_{1/2,red}$, *vs.* Fc+/Fc [32].
[g] Calculated from $E_g^{el}(eV) = E_{HOMO} - E_{LUMO}$. The optical band gap of SQ, E_g^{opt}, is larger (by 0.16 eV) than the electrochemical band gap, E_g^{el}, as observed for other squaraine dyes [34].

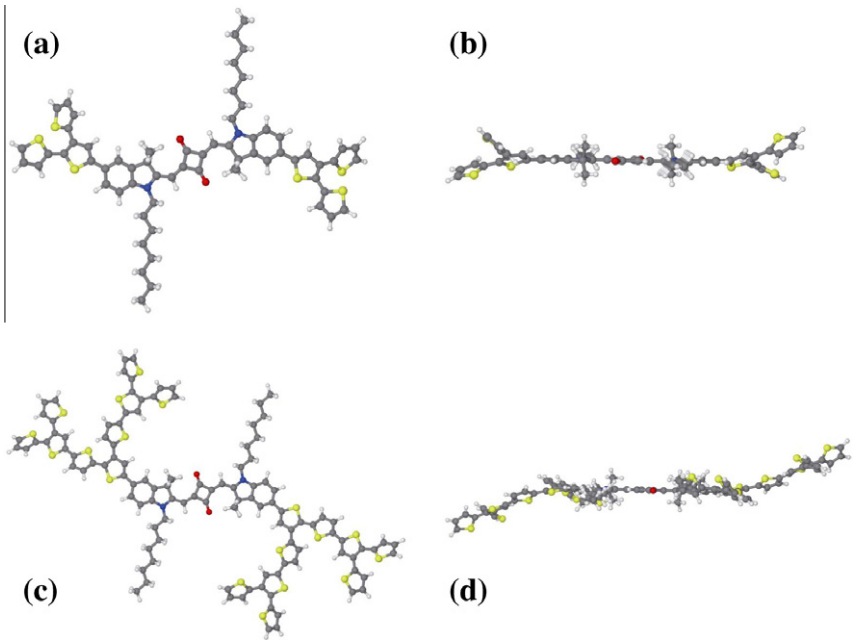

Fig. 2. Optimized structures of 6T-SQ (a front view, b side view) and 18T-SQ (c front view, d side view). Calculated energies were the same for conformations with dendrons turned by 180°.

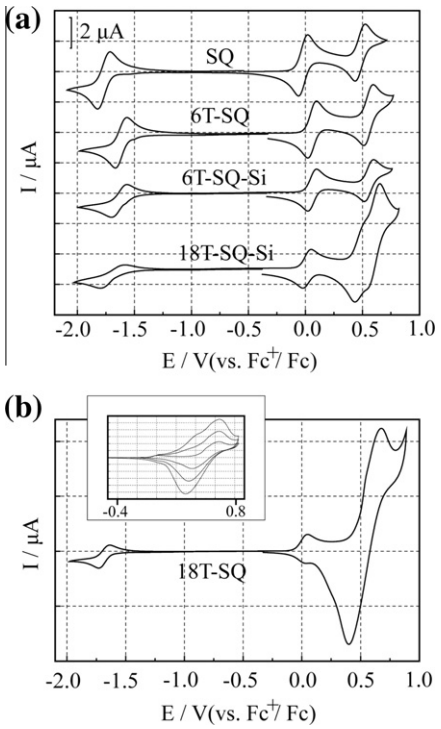

Fig. 3. (a) Cyclic voltammograms of SQ and squaraine oligothiophene hybrids. (b) First CV cycle of 18T-SQ; inset: multiple CV cycles of 18T-SQ.

mean square, rms, roughness <1 nm) films for 6T-SQ and 18T-SQ (ESI). The SQ film, on the other hand, displayed a "spherulite-type" crystalline topography (Fig. 4a). Upon annealing at ~150 °C the SQ crystals partially melted again and isolated dye clusters formed on the glass/PEDOT:PSS substrate (ESI). A pronounced crystallization was also observed for non-annealed SQ films after storage at ambient air humidity for 2 months (ESI). From this we conclude that besides $CHCl_3$ (see above) also water vapor induces SQ reorganization into more stable crystallites at rt. Isolated crystals also formed for 6T-SQ films after storage at ambient air humidity, but 18T-SQ remained completely amorphous (ESI).

Fig. 4b demonstrates the irregular 6T-SQ film morphology after heat treatment, where large crystalline domains co-exist with visually amorphous regions. The UV–vis absorption of Fig. 1b, spectrum e, was measured on a crystallized film spot size, while the spectrum c of Fig. 1b was measured on an unchanged film area. The film 18T-SQ again remained unchanged upon annealing (ESI).

DSC was measured for the pure dyes (ESI). SQ was a crystalline material with a melting temperature of 161.1 °C ($\Delta H = 83\ J\ g^{-1}$). During the heating step, the recrystallization transition occurred at 102.0 °C. This transition was already visible during the cooling cycle using a slower rate of 5 °C min^{-1}. No phase transition was observed for 18T-SQ, confirming the suppressed crystallization. For 6T-SQ, three phase transitions were observed at 51.6 °C, 62.1 °C ($\Delta H = 37\ J\ g^{-1}$) and 98.0 (small) °C upon heating. The material crystallized during the cooling cycle at 55.1 and 43.8 °C.

Blending the dyes with PCBM changed their film formation and crystallization behavior. Initially smooth films could be fabricated in all cases, even for the dye SQ that crystallizes when coated undiluted from $CHCl_3$. Storage at ambient air humidity induced limited crystallization in the SQ: PCBM film, but 6T-SQ: PCBM and 18T-SQ: PCBM

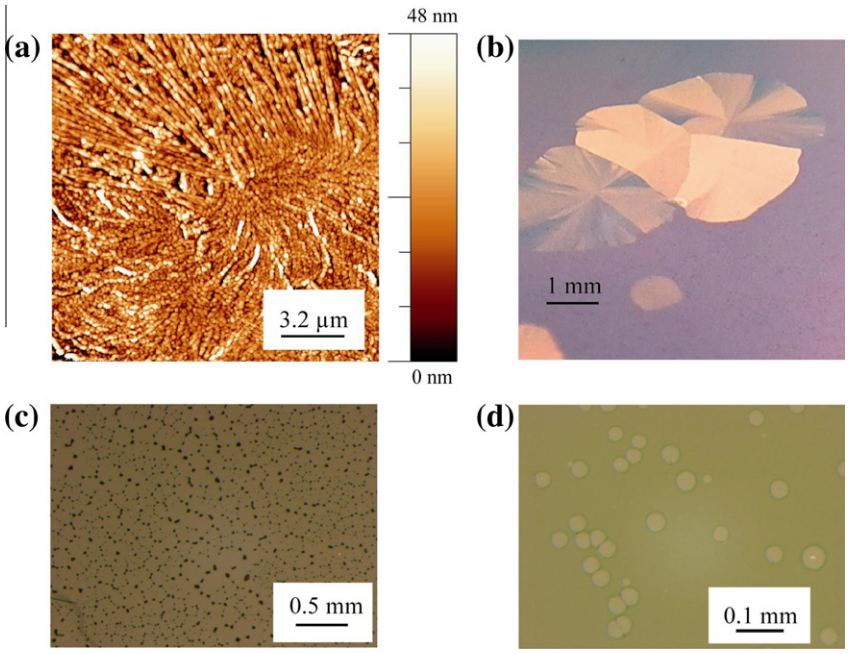

Fig. 4. (a) AFM topographical image of spin-coated SQ film, measured after storage for 2 days at room temperature under nitrogen; Optical microscope images of (b) 6T-SQ film, (c) SQ: PCBM blend film, and (d) 6T-SQ: PCBM blend film, in each case after annealing at ~150 °C for 30 min.

films remained amorphous (ESI). Also upon annealing, crystallization was suppressed for all dyes (Fig. 4c and d) and high resolution AFM scans did not show distinct signs of small-scale phase separation. No detailed information on the vertical arrangement between the dyes and PCBM through the film can be extracted from these observations alone. However, the largely reduced crystallization tendency would be consistent with the existence of an attractive interaction between the dyes and PCBM, resulting in films where the two components remain blended. That view is supported by the complete quenching of the 6T-SQ fluorescence upon mixing with PCBM (ESI), and from DSC measurements carried out for SQ: PCBM mixtures. For PCBM contents of 10 and 20 wt.% in the blends, a small SQ melting transition (at 152.9 and 150 °C, respectively) was still observed. For higher PCBM fractions in the blends, however, the crystallization of SQ was inhibited and no phase transition was measured (data not shown).

Annealing though introduced another unwanted effect and blend films were dewetting from the substrate. After 30 min of annealing at 150 °C, the blend film SQ:PCBM shows a pattern characteristic to a late stage of dewetting (droplet phase, Fig. 4c) while 6T-SQ:PCBM shows a pattern characteristic to an early dewetting stage (hole growth, Fig. 4d) [40]. The film of 18T-SQ: PCBM was the most stable in that configuration, since after annealing the film did not show signs of dewetting (ESI). It is finally interesting to note that also in bilayer 6T-SQ/C_{60} films dye crystallization was suppressed upon annealing (as demonstrated for pure 6T-SQ in Fig. 4b) and the film remained visually amorphous. A possible explanation is that C_{60} intermixes with 6T-SQ to some extent upon evaporation and this also seems to hinder dye crystallization [41].

3.2. Organic solar cells

SQ, 6T-SQ and 18T-SQ were tested with PCBM in bulk heterojunction (BHJ) solar cells. Films with thicknesses of ~90 nm (for SQ), ~70 nm (for 6T-SQ) and ~85 nm (for 18T-SQ) were spin coated from $CHCl_3$ solutions containing 3 mM of dye and 5 mg mL^{-1} PCBM. As top electrode, 40 nm of aluminium was evaporated. These as prepared solar cells did not show clear diode characteristics (performance data of all solar cells are summarized in the ESI section). The same was observed when increasing the PCBM (to 12 mg mL^{-1}) or dye concentrations (to ~5–6 mM), or when using chlorobenzene as solvent.

BHJ solar cell performance developed slightly after annealing. For 6T-SQ:PCBM before annealing, we measured (using 100 mW cm^{-2} simulated sunlight) 1.3 mA cm^{-2} for the short-circuit current (J_{sc}), 0.1 V for the open-circuit voltage (V_{oc}) and 25% for the fill factor (*FF*), resulting in η = 0.03%. After annealing, J_{sc} = 1.7 mA cm^{-2}, V_{oc} = 0.39 V, *FF* = 38%, η = 0.25% were obtained. Comparable values were measured for a 18T-SQ: PCBM cell after annealing (J_{sc} = 1.0 mA cm^{-2}, V_{oc} = 0.52 V, *FF* = 31%, η = 0.16%). None of these methods induced any mentionable performance (η < 0.04%) in SQ: PCBM BHJ solar cells.

Bilayer dye/C_{60} devices were also fabricated. $CHCl_3$ solutions containing 1.9 mM of SQ, 6T-SQ and 18T-SQ were spin coated to produce ~20 nm thick dye films. Layers of C_{60} (~40 nm), Alq_3 (~2.5 nm) and Al (~40 nm) were subsequently evaporated. The *J–V* characteristics of these solar cells are displayed in Fig. 5a using 50 mW cm^{-2} simulated sunlight, but performances were the same for 1 sun light intensity. The performances of 6T-SQ and 18T-SQ were rather similar (6T-SQ: J_{sc} = 3.2 mA cm^{-2}, V_{oc} = 0.5 V,

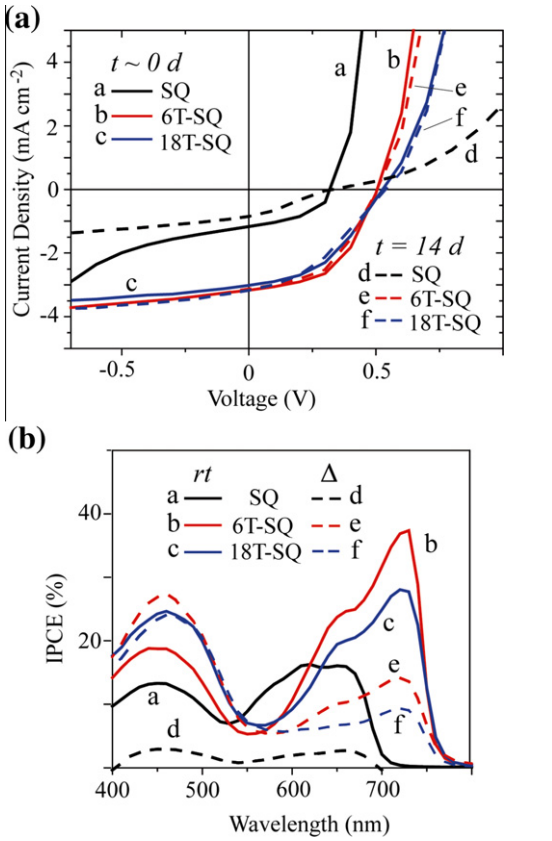

Fig. 5. (a) *J–V* characteristics (50 mW cm^{-2}) of bilayer dye(20 nm)/C_{60}(40 nm) solar cells; solid lines from as prepared cells, dashed lines after storage for 2 weeks under nitrogen. (b) Incident photon-to-electron conversion efficiencies (IPCE) of bilayer dye(20 nm)/C_{60}(40 nm) solar cells; solid lines from as prepared cells, dashed lines after heating to ~120 °C for 30 min.

FF = 50%, η = 1.6%, ½ sunlight; 18T-SQ: η = 1.4%) and did not change markedly over a period of 2 weeks of storage in the glove box. The initial SQ solar cell performed less (J_{sc} = 1.2 mA cm^{-2}, V_{oc} = 0.32 V, *FF* = 45%, η = 0.3%), and degraded further during storage (Fig. 5a, black dashed line d). To ensure a uniform dye coating, thinner films than 20 nm were not prepared. We observed that the performance decreased quickly for thicker films, mainly due to a collapse of the cell fill factor, suggesting limited hole transport through the dye film.

Annealing accelerated the degradation of SQ bilayer cells and the *J–V* characteristic was short-circuited (data not shown). For 6T-SQ and 18T-SQ, V_{oc} and *FF* remained almost constant after heating, but J_{sc} decreased by ~25%. Fig. 5b shows the corresponding IPCE curves before (solid lines) and after heating (dashed lines). Comparing the IPCE for SQ before (curve a) and after annealing (curve d), cell degradation gets evident. For 6T-SQ and 18T-SQ, annealing induced a marked decrease of the IPCE in the wavelength region where the squaraine core absorbs, but remains constant below ~550 nm for 18T-SQ and even slightly increases for 6T-SQ. Note that the curves in the wavelength region between 400 and ~550 nm are probably the sum of overlapping photocurrents generated after excitation of C_{60}, and from charge-transfer induced by direct excitation of the oligothiophene dendrons.

4. Discussion

Thin film formation and bilayer OPV performance using SQ is characterized by a pronounced crystallization tendency of the dye. An initial precipitation of dye crystals out of the solvent-quenched film is suggested from UV–vis spectroscopy at rt (Fig. 1b), and results of SQ/C_{60} OPV cells showed that the film morphology develops further over a period of several weeks (Fig. 5a). Therefore, meaningful solar cell data can only be obtained after an extended storage period, at least for the squaraine dye we studied here. Heat treatment of SQ films induced reorganization into large crystallites, resulting in discontinuous films and associated poor OPV performance.

The oligothiophene dendrons in the 6T-SQ and 18T-SQ hybrids seem to serve a dual function. Firstly, they contribute to light absorption in the 300–500 nm wavelength range, and (the albeit limited) conjugation with the squaraine core leads to a red shift of the dye absorption. Secondly, the dendrons substantially hinder the squaraine core crystallization. This gets more pronounced with increasing dendron size, and 18T-SQ films showed no macroscopic crystallites after initial coating and heat treatment. In addition, bilayer 6T-SQ and 18T-SQ OPV cells were stable upon rt storage (Fig. 5a), but performance degraded after heat treatment, mainly because of a decrease of the photocurrent produced after photoexcitation of the squaraine moiety (Fig. 5b). For pure 6T-SQ films, isolated crystallization upon cooling from the melt was evident (Fig. 4b), but we note that the extent of crystallization can be different in the actual solar cell geometry, where 6T-SQ is covered by an additional C_{60}/Al layer. The performance decrease upon annealing is consistent with dye aggregation/crystallization, with an associated demixing and reduction of the diffuse squaraine core donor–fullerene acceptor zone formed upon initial C_{60} evaporation [41,42]. Since C_{60} has a substantially larger exciton diffusion length than squaraines (~40 nm [43] *vs.* smaller than ~5 nm [19,23]), the relative decrease of the IPCE after squaraine excitation is larger than in the wavelength region where C_{60} absorbs. Details for the short wavelength IPCE increase in 6T-SQ/C_{60} solar cells after annealing are unknown, but possible reasons might be the formation of a more ordered dendron morphology or a closer proximity between C_{60} and the thiophenes, allowing for more charge generation and facilitated hole transport through the dye film. Further details of the thermotropic behavior of 6T-SQ were not studied within the scope of this work.

For films from blend solutions, microscopy, DSC and AFM data do not reveal a clear picture if or to what extent phase separation between the squaraines and PCBM occurs. Similar results have been reported for other small molecule: fullerene blends [44]. No or unincisive phase separation persisting through the film is consistent with the measurement of pronounced dye fluorescence quenching in the blend, and the observation that efficiencies of as-prepared BHJ cells were low. It is generally accepted that

for a BHJ system an optimal length scale of the phase-separated domains exist. Below that length scale performance is hampered by reduced hole and electron mobility and missing continuous channels for efficient charge transport to the electrodes, above that length scale the interfacial area between donor and acceptor is small [45]. Annealing improved the performance of 6T-SQ and 18T-SQ: PCBM cells to some extent, suggesting that the components start to demix. However, we observed dewetting of the films at elevated temperatures. For SQ: PCBM blends, dewetting seems to be dominating, and no working solar cells could be fabricated.

These results should be compared with reported work on squaraine–fullerene OPV cells. Unsymmetrical squaraines have been applied in one example in bilayer squaraine/C_{60} OPV devices [17]. It was found that η values increased for thinner dye films (η = 1.01% for a 20 nm thick squaraine layer), due to a combination of very high dye light extinction coefficient, small exciton diffusion length and limited hole transport through the squaraine film, as inferred from the low cell fill factors (*FF* < 35%). A squaraine: PCBM BHJ solar cell has been reported in 2008 [15]. Again, η values increased with decreasing film thickness, and η = 1.24% (*FF* < 40% throughout) was obtained when spin coating a 30 nm thick film using a 1:3 (wt:wt) squaraine: PCBM mixture in $CHCl_3$. Subsequently, the hole transport mobility could be improved by replacing the squaraine alkyl side chains by a hexenyl group, with η increasing to 1.99% (albeit using $PC_{70}BM$ as acceptor at the same time, *FF* < 40%) [16].

The 2,4-bis[4-(*N*,*N*-diisobutylamino)-2,6-dihydroxyphenyl] squaraine compound has been studied in detail [18–21]. A squaraine/C_{60} bilayer cell was fabricated by thermal evaporation [18]. The highest performance (η = 3.1%) was measured for the thinnest (6.5 nm) squaraine film, and the trends for J_{sc} and *FF* as function of squaraine thickness (6.5–20 nm) were consistent with increased resistance of hole transport in thicker dye films. Squaraine films of comparable thickness (6.2 nm) were also prepared by spin coating [19]. Before evaporating the C_{60} acceptor, the dye films were converted from amorphous to polycrystalline via postannealing at elevated temperature. This roughened the squaraine film surface, and increased the exciton diffusion length and film conductivity. C_{60} evaporation resulted in a layered, controlled BHJ device structure, with an optimized performance of η = 4.6%. Using the same squaraine, solution-processed BHJ with various relative dye: $PC_{70}BM$ concentrations were fabricated [20]. Performances increased with increasing fullerene content, and η = 2.7% was measured for a 1:6 squaraine:$PC_{70}BM$ blend mixture. Low squaraine concentrations, however, affected the hole mobility, resulting in unbalanced electron and hole transport and relatively low (<40%) *FF*. Finally, solvent (dichloromethane) annealing of these squaraine: $PC_{70}BM$ (1:6) films created continuous squaraine crystalline and low-resistive pathways for hole conduction, and η increased to 5.2% [21]. Further improvements have been achieved by substituting the *N*-alkyl groups with arylamine groups, and $\eta = 5.7 \pm 0.6\%$ has been reported for functionalized squaraine/C_{60} solar cells only recently [46].

In these studies, solar cells performed better using thinner films. This is consistent with our results. The high light absorption coefficients of squaraines allowed the use of very thin films that are necessary to compensate for the small exciton diffusion length and conductivity. One potential issue might be the pinhole-free deposition of ultrathin films over larger areas in up scaled solar cells, but such data have not been published so far. Fine tuning of the squaraine crystallinity via solvent or temperature annealing was found to be beneficial, since this increased the hole conduction mobility and the exciton diffusion length, and provided nanoscale mixtures with dimensions that lie within the diffusion length of the exciton generation sites. Excessive heat treatment or solvent annealing times, however, resulted in discontinuous films and pinholes between the active layer and the electrodes, leading to shorted solar cells.

5. Conclusions

The main motivation for the synthesis of molecular push–pull systems so far was the adjustment of the optical and electronic properties of the electron-donating component. We demonstrate here that oligothiophene dendrons attached to a squaraine dye in addition have a pronounced and beneficial influence on the developing thin-film morphology. Therefore, such decorating moieties of a central light-absorbing core unit can be used both to adjust optoelectronic and morphological film properties at the same time. Similar synthetic strategies might be of relevance for other small molecular semiconductors with a strong tendency towards crystallization.

Our results agree with recent work on squaraine dyes for organic solar cell applications. The promising results using simple bilayer devices with a small interfacial donor–acceptor area demonstrated the potential of the fullerene–squaraine material system. A challenge for the further development is therefore the fabrication of optimized blend film morphologies. The squaraine core crystallization tendency may be further suppressed by introducing bulkier side groups than the straight C8 chains used here. Recently, it has been realized that the chemical nature and position of solubilizing side chains play an important role not only on the thin-film morphology, but also on the electronic processes and the performance of organic solar cells [46,47]. The use of larger oligothiophene dendrons, however, seems not to be necessary, and is also not required for increased conjugation lengths, since the electronic communication between the donor and acceptor units is limited to a few thiophene units.

Acknowledgements

We thank D. Passerone (Empa) for help with molecular modeling calculations, U. Müller (Empa) and the Swiss Scanning Probe Microscopy User Laboratory (Empa) for AFM support, and C. Walter and B. Fischer for help with DSC measurements. This work was supported by NPL, Empa, and the Deutsche Forschungsgemeinschaft (DFG

SPP1355). YZ thanks "the Global COE Program" from MEXT Japan for financial support.

Appendix A. Supplementary data

Supplementary data associated with this article can be found, in the online version, at http://dx.doi.org/10.1016/j.orgel.2012.03.022.

References

[1] C. Brabec, V. Dyakonov, U. Scherf (Eds.), Organic Photovoltaics, Wiley-VCH, Weinheim, Germany, 2008.
[2] Y. Liang, Z. Xu, J. Xia, S.-T. Tsai, Y. Wu, G. Li, C. Ray, L. Yu, Adv. Mater. 22 (2010) E135.
[3] B. Walker, C. Kim, T.-Q. Nguyen, Chem. Mater. 23 (2011) 470.
[4] J. Roncali, Acc. Chem. Res. 42 (2009) 1719.
[5] A.W. Hains, Z. Liang, M.A. Woodhouse, B.A. Gregg, Chem. Rev. 110 (2010) 6689.
[6] B. Walker, A.B. Tamayo, X.-D. Dang, P. Zalar, J.H. Seo, A. Garcia, M. Tantiwiwat, T.-Q. Nguyen, Adv. Funct. Mater. 19 (2009) 3063.
[7] H. Shang, H. Fan, Y. Liu, W. Hu, Y. Li, X. Zhan, Adv. Mater. 23 (2011) 1554.
[8] Y. Liu, X. Wan, F. Wang, J. Zhou, G. Long, J. Tian, J. You, Y. Yang, Y. Chen, Adv. Energy Mater. 1 (2011) 771.
[9] S. Roquet, A. Cravino, P. Leriche, O. Alévêque, P. Frère, J. Roncali, J. Am. Chem. Soc. 128 (2006) 3459.
[10] J. Mei, K.R. Graham, R. Stalder, J.R. Reynolds, Org. Lett. 12 (2010) 660.
[11] Y. Li, Q. Guo, Z. Li, J. Pei, W. Tian, Energy Environ. Sci. 3 (2010) 1427.
[12] A. Mishra, C.-Q. Ma, P. Bäuerle, Chem. Rev. 109 (2009) 1141.
[13] J.-Y. Li, C.-Y. Chen, C.-P. Lee, S.-C. Chen, T.-H. Lin, H.-H. Tsai, K.-C. Ho, C.-G. Wu, Org. Lett. 12 (2010) 5454.
[14] S. Paek, H. Choi, C. Kim, N. Cho, S. So, K. Song, M.K. Nazeeruddin, J. Ko, Chem. Commun. 47 (2011) 2874.
[15] F. Silvestri, M.D. Irwin, L. Beverina, A. Facchetti, G.A. Pagani, T.J. Marks, J. Am. Chem. Soc. 130 (2008) 17640.
[16] D. Bagnis, L. Beverina, H. Huang, F. Silvestri, Y. Yao, H. Yan, G.A. Pagani, T.J. Marks, A. Facchetti, J. Am. Chem. Soc. 132 (2010) 4074.
[17] B. Fan, Y. Maniglio, M. Simeunovic, S. Kuster, T. Geiger, R. Hany, F. Nüesch, Int. J. Photoenergy (2009) 581068.
[18] S. Wang, E.I. Mayo, M.D. Perez, L. Griffe, G. Wei, P.I. Djurovich, S.R. Forrest, M.E. Thompson, Appl. Phys. Lett. 94 (2009) 233304.
[19] G. Wei, R.R. Lunt, K. Sun, S. Wang, M.E. Thompson, S.R. Forrest, Nano Lett. 10 (2010) 3555.
[20] G. Wei, S. Wang, K. Renshaw, M.E. Thompson, S.R. Forrest, ACS Nano. 4 (2010) 1927.
[21] G. Wei, S. Wang, K. Sun, M.E. Thompson, S.R. Forrest, Adv. Energy Mater. 1 (2011) 184.
[22] U. Mayerhöffer, K. Deing, K. Gruß, H. Braunschweig, K. Meerholz, F. Würthner, Angew. Chem. Int. Ed. 48 (2009) 8776.
[23] B.E. Lassiter, G. Wei, S. Wang, J.D. Zimmerman, V.V. Diev, M.E. Thompson, S.R. Forrest, Appl. Phys. Lett. 98 (2011) 243307.
[24] A.D. Becke, J. Chem. Phys. 98 (1993) 5648.
[25] M. Valiev, E.J. Bylaska, N. Govind, K. Kowalski, T.P. Straatsma, H.J.J. Van Dam, D. Wang, J. Nieplocha, E. Apra, T.L. Windus, W.A. De Jong, Comp. Phys. Commun. 181 (2010) 1477.
[26] W. Humphrey, A. Dalke, K. Schulten, J. Mol. Graphics 14 (1996) 33.
[27] S. Kuster, T. Geiger, Dyes and Pigments, submitted for publication.
[28] C.-Q. Ma, E. Mena-Osteritz, M. Wunderlin, G. Schulz, P. Bäuerle, Chem. Eur. J. 2012, http://dx.doi.org/10.1002/chem.201200231.
[29] D. Scherer, R. Dörfler, A. Feldner, T. Vogtmann, M. Schwoerer, U. Lawrentz, W. Grahn, C. Lambert, Chem. Phys. 279 (2002) 179.
[30] S.F. Völker, S. Uemura, M. Limpinsel, M. Mingebach, C. Deibel, V. Dyakonov, C. Lambert, Macromol. Chem. Phys. 211 (2010) 1098.
[31] W.W.H. Wong, C.-Q. Ma, W. Pisula, C. Yan, X. Feng, D.J. Jones, K. Müllen, R.A.J. Janssen, P. Bäuerle, A.B. Holmes, Chem. Mater. 22 (2010) 457.
[32] C.M. Cardona, W. Li, A.E. Kaifer, D. Stockdale, G.C. Bazan, Adv. Mater. 23 (2011) 2367.
[33] T. Johansson, W. Mammo, M. Svensson, M.R. Andersson, O. Inganäs, J. Mater. Chem. 13 (2003) 1316.
[34] T. Geiger, S. Kuster, J.-H. Yum, S.-J. Moon, M.K. Nazeeruddin, M. Grätzel, F. Nüesch, Adv. Funct. Mater. 19 (2009) 2720.
[35] P. Sonar, H. Benmansour, T. Geiger, A.D. Schlüter, Polymer 48 (2007) 4996.
[36] C.-Q. Ma, W. Pisula, C. Weber, X.-L. Feng, K. Müllen, P. Bäuerle, Chem. Eur. J. 17 (2011) 1507.
[37] A. Ajayaghosh, Chem. Soc. Rev. 32 (2003) 181.
[38] L. Chang, H.W.A. Lademann, J.-B. Bonekamp, K. Meerholz, A.J. Moulé, Adv. Funct. Mater. 21 (2011) 1779.
[39] B.J. Schwartz, Ann. Rev. Phys. Chem. 54 (2003) 141.
[40] G. Reiter, Phys. Rev. Lett. 68 (1992) 75.
[41] W. Kylberg, P. Sonar, J. Heier, J.-N. Tisserant, C. Müller, F. Nüesch, Z.-K. Chen, A. Dodabalapur, S. Yoon, R. Hany, Energy Environ. Sci. 4 (2011) 3617.
[42] F.A. Castro, H. Benmansour, C.F.O. Graeff, F. Nüesch, E. Tutis, R. Hany, Chem. Mater. 18 (2006) 5504.
[43] P. Peumans, A. Yakimov, S.R. Forrest, J. Appl. Phys. 93 (2003) 3693.
[44] A. Tamayo, T. Kent, M. Tantitiwat, M.A. Dante, J. Rogers, T.-Q. Nguyen, Energy Environ. Sci. 2 (2009) 1180.
[45] P.K. Watkins, A.B. Walker, G.L.B. Verschoor, Nano Lett. 5 (2005) 1814.
[46] G. Wei, X. Xiao, S. Wang, K. Sun, K.J. Bergemann, M.E. Thompson, S.R. Forrest, ACS Nano. 6 (2012) 972.
[47] S. Massip, P.M. Oberhumer, G. Tu, S. Albert-Seifried, W.T.S. Huck, R.H. Friend, N.C. Greenham, J. Phys. Chem. C 115 (2011) 25046.